

An estimation of the effective number of electrons contributing to the coordinate measurement with a TPC

II

Makoto Kobayashi

High Energy Accelerator Research Organization (KEK), Tsukuba, 305-0801, Japan

Abstract

For time projection chambers (TPCs) the accuracy in measurement of the track coordinates along the pad-row direction deteriorates with the drift distance (z): $\sigma_X^2 \sim D^2 \cdot z/N_{\text{eff}}$, where D is the diffusion constant and N_{eff} is the effective number of electrons. Experimentally it has been shown that N_{eff} is smaller than the average number of drift electrons per pad row ($\langle N \rangle$). In the previous work we estimated N_{eff} by means of a simple numerical simulation for argon-based gas mixtures, taking into account the diffusion of electrons only in the pad-row direction [1]. The simulation showed that N_{eff} could be as small as $\sim 30\%$ of $\langle N \rangle$ because of the combined effect of statistical fluctuations in the number of drift electrons (N) and in their multiplication in avalanches. In this paper, we evaluate the influence of the diffusion normal to the pad-row direction on the effective number of electrons. The de-clustering of the drift electrons due to the diffusion makes N_{eff} drift-distance dependent. However, its effect was found to be too small to explain the discrepancy between the values of N_{eff} measured with two TPC prototypes different in size.

Keywords:

TPC, Resolution, Effective Number of Electrons, Diffusion, Declustering, Simulation, MPGD, ILC
PACS: 29.40.Cs, 29.40.Gx

1. Introduction

In the previous paper we estimated the effective number of electrons (N_{eff}) contributing to the coordinate measurement of a time projection chamber (TPC) equipped with a Micro-Pattern Gaseous Detector (MPGD) and ideal readout electronics [1]. N_{eff} parametrizes the spatial resolution for a pad row as follows

$$\sigma_X^2 = \sigma_{X0}^2 + \frac{D^2}{N_{\text{eff}}} \cdot z \quad (1)$$

where σ_X is the spatial resolution along the pad-row direction, σ_{X0} is the intrinsic resolution, and D denotes the transverse diffusion constant, with z being the drift distance. In the ideal case (with an infinitesimal pad pitch) σ_{X0} vanishes for particle tracks perpendicular to the pad row, and increases with the track angle (ϕ) with respect to the pad-row normal because of the angular pad effect. Only right angle tracks ($\phi = 0^\circ$) are considered throughout the present work.

Under the conditions listed in Ref. [1], N_{eff} is given by

$$\frac{1}{N_{\text{eff}}} = \left\langle \frac{1}{N} \right\rangle \cdot (1 + f) \quad (2)$$

where N denotes the total number of drift electrons detected by the pad row and f is the relative variance of the gas-amplified signal charge (q) induced on the pad row by single drift electrons (avalanche fluctuation: $\sigma_q^2/\langle q \rangle^2$)¹. Although Eq. (2) was derived assuming the total charge ($\sum_{i=1}^N q_i$) to be constant ($N \cdot \langle q \rangle$) it was found to be a good approximation by a numerical simulation for a practical value of $\langle N \rangle$ (see Ref. [1], and Appendix A for details).

The simulation for argon-based gas mixtures gave N_{eff} of ~ 22 for $f = 2/3$ and a pad-row pitch of 6.3 mm [1], which is about 30% of the average value of N ($\langle N \rangle \sim 71$), and is consistent with the values obtained with a small prototype TPC [3–5]. The value of N_{eff} corresponds to ~ 36 for a pad-row pitch normalized to 1 cm, assuming N_{eff} to be (approximately) proportional to the pad-row pitch².

Recent resolution measurements with a larger prototype TPC with MicroMEGAS readout, however, gave a significantly larger estimate for N_{eff} (~ 56 for 1-cm pad height) [6]³. A possible origin of the discrepancy could be the de-clustering of drift electrons due to diffusion normal to the pad-row direction (D_y), which is expected to be more efficient for larger TPCs with a longer average drift distance. It should be pointed out that the diffusion only along the pad-row direction (D_x) was taken into account in Ref. [1]. In the present work, we evaluate the contribution of the de-clustering effect to the increase of N_{eff} , through the decrease of $\langle 1/N \rangle$ due to the finite D_y , in argon-based gas mixtures.

An analytic and qualitative approach is described through Section 2 to 4, the results of a numerical simulation are shown in Section 5, and Section 6 concludes the paper. Readers are suggested to read Ref. [1] in advance.

2. Long drift-distance limit

Let us consider the hypothetical case of a TPC with an infinitely large drift distance⁴. Primary ionization clusters created along a particle track at an infinitely large drift distance get completely de-clustered, and the secondary electrons distribute uniformly and randomly on the readout plane. They no longer have any information on the original cluster positions. Therefore the total number of drift electrons reaching a pad row obeys Poisson statistics with a mean $\mu = \langle N \rangle$:

$$P(N) = e^{-\mu} \cdot \frac{\mu^N}{N!}.$$

The average value of the inverse of N in this case is given by

$$\begin{aligned} \left\langle \frac{1}{N} \right\rangle &= \frac{1}{1 - e^{-\mu}} \cdot \sum_{N=1}^{\infty} \frac{1}{N} \cdot P(N) \\ &= \frac{e^{-\mu}}{1 - e^{-\mu}} \cdot \sum_{N=1}^{\infty} \frac{\mu^N}{N \cdot N!} \\ &= \frac{e^{-\mu}}{1 - e^{-\mu}} \cdot (E_i(\mu) - \ln(\mu) - \gamma) \end{aligned}$$

¹ It should be noted that Eq. (2) is an expression for $1/N(h)$ in Eq. (7.33) of Ref. [2].

² Actually, this is a bold assumption. See Appendix A.

³ In fact, the values of N_{eff} were obtained using different kinds of charged particle: a beam of 5-GeV/ c electrons in Ref. [6] while a beam of 4-GeV/ c pions or cosmic rays in Refs. [3–5]. The discrepancy is still large, however, even if the difference in the primary ionization density is taken into account.

⁴ The dimensions of the readout pad plane are considered to be infinitely large as well. Otherwise a part of the drift electrons created at long drift distances would be absorbed by the field cage (the inner or outer wall of a cylindrical TPC) before reaching the readout plane.

where E_i is the exponential integral⁵ and γ is the Euler-Mascheroni constant (~ 0.577). When $N = 0$ the pad row is inefficient and provides no coordinate measurement. Therefore it is excluded from the summation. Fig. 1 shows the behavior of $R_N \equiv \langle N \rangle \cdot \langle 1/N \rangle$ as a function of $\langle N \rangle$. For a practical value of $\langle N \rangle \gtrsim 50$, $\langle 1/N \rangle \sim 1/\langle N \rangle$ and N_{eff} is expected to be $\sim \langle N \rangle / (1 + f)$ at an infinitely long drift distance.

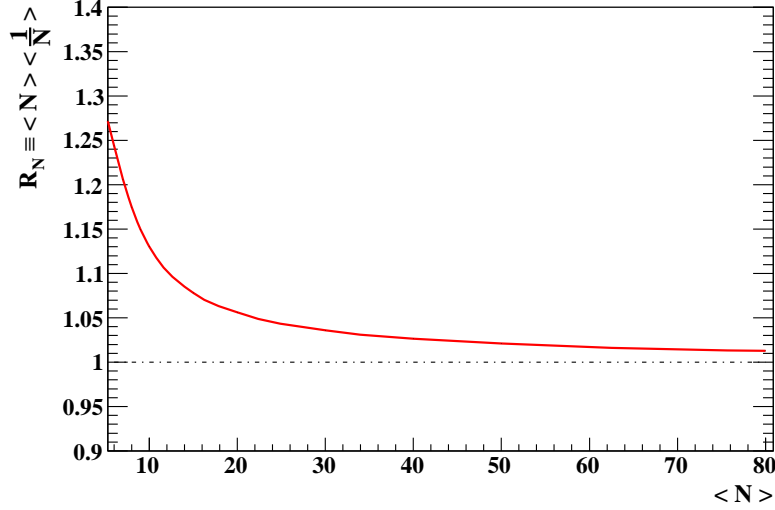


Figure 1: $R_N \equiv \langle N \rangle \cdot \langle 1/N \rangle$ as a function of the average number of electrons in the case of Poisson distribution for N .

3. Short drift-distance limit

At zero drift distance, where the clusters are intact, the N -distribution is a Landau type with a long tail for large N due to occasional large clusters. For the Landau distribution, the mode (\hat{N}) is considerably smaller than the average ($\langle N \rangle$), whereas $\langle 1/N \rangle$ is close to $1/\hat{N}$ (see, for example, Fig. 5 and 6 in Ref. [1]). Therefore R_N defined above is significantly larger than unity even for relatively large $\langle N \rangle$ and $N_{\text{eff}} = \langle N \rangle / (1 + f) / R_N < \langle N \rangle / (1 + f)$.

As the clusters disintegrate with the increase of drift distance, the N -distribution changes its shape because of the diffusion normal to the pad-row direction, approaching a Poissonian, for which $\hat{N} \sim \langle N \rangle^6$. With the progress of de-clustering \hat{N} shifts towards $\langle N \rangle$, therefore $\langle 1/N \rangle$ decreases, while $\langle N \rangle$ remains constant⁷. Consequently, N_{eff} is expected to be an increasing function of the drift distance, with an asymptotic maximum of $\sim \langle N \rangle / (1 + f)$.

The rate at which the Landau distribution approaches a Poissonian with the increase of drift distance depends on the pad height, the diffusion constant, and the cluster size distribution. In the next section, the change in the variance of the N -distribution is calculated in order to demonstrate that the transition to the Poissonian is slow.

⁵ The exponential integral is defined as

$$E_i(x) = \int_{-\infty}^x \frac{e^t}{t} dt .$$

⁶ A Poissonian with $\langle N \rangle \gtrsim 20$ is close to a Gaussian.

⁷ The most probable energy loss measured with a pad row is therefore expected to increase gradually with the drift distance.

4. Variance of the N -distribution

We evaluate in this section the variance (Var) of the total number of electrons reaching a readout pad row (N) since $\text{Var}(N)$ gives a good measure for the deviation of the N -distribution from a Poissonian, for which $\text{Var}(N) = \langle N \rangle$. First, let us suppose that a single point-like electron cluster of size n is created at a coordinate $y = Y$ in the direction of the pad-row normal and $z = Z$ in the drift direction, measured from the readout plane. The electrons diffuse on their way towards the readout plane. Their spread in the y -coordinate is given by a Gaussian with a standard deviation of $\sigma \equiv \sigma_y = D \cdot \sqrt{Z}$, at the pad rows with a height of h ⁸. The probability to find ν electrons reaching the pad row is given by⁹

$$P(\nu; Y, \sigma) = \binom{n}{\nu} \cdot \Pi^\nu(Y) \cdot (1 - \Pi(Y))^{n-\nu}$$

where

$$\Pi(Y) = \int_{-h/2}^{h/2} G(y; Y, \sigma) dy$$

with

$$G(y; Y, \sigma) \equiv \frac{1}{\sqrt{2\pi}\sigma} \cdot \exp\left[-\frac{(y - Y)^2}{2\sigma^2}\right].$$

Since $P(\nu; Y, \sigma)$ represents a binomial statistics for a fixed Y (and σ), $\langle \nu \rangle$ and $\langle \nu^2 \rangle$ are given by

$$\langle \nu(Y) \rangle = n \cdot \Pi(Y)$$

and

$$\langle \nu^2(Y) \rangle = n \cdot \Pi(Y) + n(n - 1) \cdot \Pi^2(Y).$$

Let us further assume that the initial cluster is randomly created in a y -region $[-H/2, +H/2]$ with $H \gg \sigma$ (see Fig. 2). Then, averaging over $-H/2 \leq Y \leq +H/2$,

$$\begin{aligned} \langle \nu \rangle &= \frac{1}{H} \int_{-H/2}^{H/2} \langle \nu(Y) \rangle dY \\ &= \frac{n}{H} \int_{-H/2}^{H/2} dY \int_{-h/2}^{h/2} G(y; Y, \sigma) dy \\ &= \frac{n}{H} \int_{-h/2}^{h/2} dy \int_{-H/2}^{H/2} G(y; Y, \sigma) dY \\ &\sim \frac{n \cdot h}{H} \\ \text{Var}(\nu) &= \frac{1}{H} \int_{-H/2}^{H/2} \langle \nu^2(Y) \rangle dy - \langle \nu \rangle^2 \\ &\sim \frac{n \cdot h}{H} + \frac{n(n - 1)}{H} \int_{-H/2}^{H/2} \Pi^2(Y) dY - \left(\frac{n \cdot h}{H}\right)^2 \\ &\sim \frac{n \cdot h}{H} + \frac{n(n - 1)}{H} \cdot h \cdot g\left(\frac{\sigma}{h}\right) - \left(\frac{n \cdot h}{H}\right)^2 \end{aligned}$$

⁸ More precisely h should be understood as the pad-row pitch, which is usually slightly larger than the pad height when the readout plane is covered over with pads. The pad-row pitch and the pad height (h) are not distinguished in the present paper.

⁹ Hereafter the notation $f^n(x)$ represents the n -th power of a function $f(x)$, i.e. $(f(x))^n$.

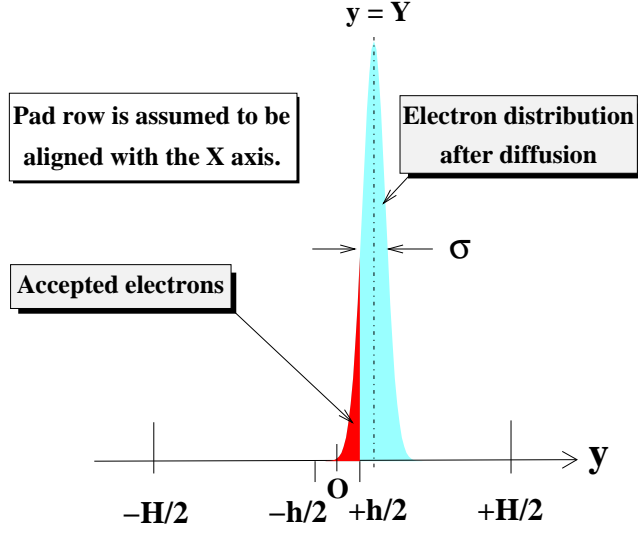


Figure 2: Illustration of the relevant variables.

where

$$g\left(\frac{\sigma}{h}\right) \equiv \operatorname{erf}\left(\frac{h}{2\sigma}\right) - \frac{2}{\sqrt{\pi}} \cdot \frac{\sigma}{h} \cdot \left[1 - \exp\left(-\frac{h^2}{4\sigma^2}\right)\right].$$

See Appendix B for the derivation of the function $g(\sigma/h)$.

If there are N_{CL} (independent) clusters in $[-H/2, +H/2]$, the average and the variance are given by multiplying N_{CL} ¹⁰:

$$\begin{aligned} \langle \nu \rangle &= \frac{N_{\text{CL}}}{H} \cdot n \cdot h \\ \operatorname{Var}(\nu) &= \frac{N_{\text{CL}}}{H} \cdot n \cdot h + \frac{N_{\text{CL}}}{H} \cdot n(n-1) \cdot h \cdot g\left(\frac{\sigma}{h}\right) - N_{\text{CL}} \cdot \left(\frac{n \cdot h}{H}\right)^2. \end{aligned}$$

Taking the limit of $H \rightarrow \infty$ while keeping the cluster density $\rho \equiv N_{\text{CL}}/H$ constant,

$$\begin{aligned} \langle \nu \rangle &= \rho \cdot n \cdot h \\ \operatorname{Var}(\nu) &= \rho \cdot n \cdot h + \rho \cdot n(n-1) \cdot h \cdot g\left(\frac{\sigma}{h}\right). \end{aligned}$$

In reality the cluster density (ρ) depends on the cluster size (n):

$$\rho = \rho(n) \equiv \rho_0 \cdot p(n)$$

¹⁰ Note that

$$\begin{aligned} \left\langle \sum_{i=1}^{N_{\text{CL}}} \nu_i \right\rangle &= N_{\text{CL}} \cdot \langle \nu \rangle \quad \text{and} \\ \left\langle \left(\sum_{i=1}^{N_{\text{CL}}} \nu_i - \left\langle \sum_{i=1}^{N_{\text{CL}}} \nu_i \right\rangle \right)^2 \right\rangle &= \left\langle \left(\sum_{i=1}^{N_{\text{CL}}} (\nu_i - \langle \nu_i \rangle) \right)^2 \right\rangle = N_{\text{CL}} \cdot \langle (\nu - \langle \nu \rangle)^2 \rangle. \end{aligned}$$

where ρ_0 is the total primary ionization density and $p(n)$ is the proportion of the cluster of size n ($\sum_n p(n) = 1$). The number of electrons detected by the pad row (N) is the sum of the contribution (ν) from various cluster sizes. Consequently, its average and variance are given by

$$\begin{aligned} \langle N \rangle &= \rho_0 \cdot h \cdot \sum_n n \cdot p(n) \\ \text{Var}(N) &= \rho_0 \cdot h \cdot \sum_n n \cdot p(n) \cdot \left(1 + (n - 1) \cdot g\left(\frac{\sigma}{h}\right) \right) . \end{aligned}$$

Fig. 3 (a) shows

$$\frac{\text{Var}(\nu)}{\langle \nu \rangle} = 1 + (n - 1) \cdot g\left(\frac{\sigma}{h}\right)$$

for several values of the cluster size n as a function of the scaling parameter σ/h . It is clear that the

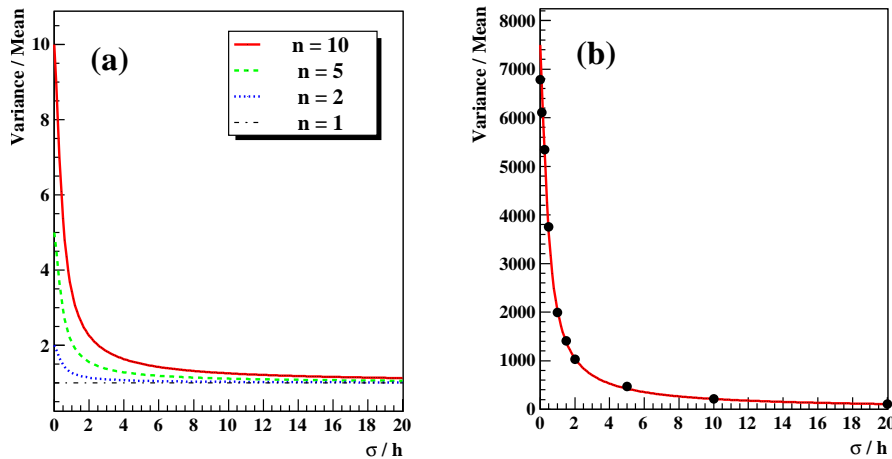


Figure 3: Variance divided by mean as a function of the scaling parameter σ/h : (a) for several fixed values of the cluster size and (b) for a realistic cluster-size distribution along with the *data points* given by a numerical simulation (filled circles).

ν distribution approaches a Poissonian ($\text{Var}(\nu)/\langle \nu \rangle = 1$) slowly with the increase of σ/h , especially for large clusters. Fig. 3 (b) shows the variance divided by the average for a realistic N -distribution:

$$\begin{aligned} \frac{\text{Var}(N)}{\langle N \rangle} &= \frac{\sum_n n \cdot p(n) \cdot \left(1 + (n - 1) \cdot g\left(\frac{\sigma}{h}\right) \right)}{\sum_n n \cdot p(n)} \\ &= 1 + \frac{\sum_n n(n - 1) \cdot p(n)}{\sum_n n \cdot p(n)} \cdot g\left(\frac{\sigma}{h}\right) , \end{aligned}$$

along with the ratios obtained with a numerical simulation (see Section 5). The probability mass function $p(n)$ was assumed to be that corresponding to the cluster-size distribution shown in Fig. 2 of Ref. [1]. It should be noted that $\text{Var}(N)/\langle N \rangle = \langle n^2 \rangle / \langle n \rangle$ whereas $\text{Var}(\nu)/\langle \nu \rangle = n$, at $\sigma/h = 0$. Consequently, the value of $\text{Var}(N)/\langle N \rangle$ at zero drift distance is rather large because of the contribution of (very) large clusters.

Fig. 3 (b) tells us that the N -distribution is a Landau type at short drift distances and approaches a Poissonian very slowly with the increase of drift distance, owing to the de-clustering. Its average ($\langle N \rangle$) remains constant during the transition.

5. Evaluation of N_{eff} by a simulation

The analytic approach described through Section 2 to 4 shows that N_{eff} is expected to be a slowly increasing function of σ/h , i.e. the drift distance. In order to confirm this quantitatively, we evaluated N_{eff} by means of a numerical simulation.

The simulation code is identical to that used in the previous work [1], except that the diffusion of drift electrons normal to the pad-row direction (D_y) is taken into account. Initial electron clusters are randomly generated along the y -axis (with the pad row aligned with the x -axis) in a range wide enough compared to the diffusion ($\sigma = D \cdot \sqrt{Z}$) and the pad height (h). The cluster density is assumed to be $24.3 \text{ cm}^{-1} \times 1.2$ (relativistic rise factor) as in the previous paper [1]. The size of each cluster is determined randomly using the probability mass function $p(n)$ (see Section 4). The secondary electrons originated from each cluster are then dispersed in the directions of the pad row (x) and the pad-row normal (y) with $\sigma_x = \sigma_y = \sigma = D \cdot \sqrt{Z}$ ¹¹. The electrons with the final position located within the pad row ($|y| \leq h/2$) are accepted (see Fig 2). Gas gain is assigned to each of the accepted electrons randomly assuming a Polya distribution ($\theta = 0.5$, corresponding to $f = 2/3$) for the avalanche fluctuation. The coordinate resolution (σ_X) is evaluated from the fluctuation in the charge centroid of the accepted electrons in the pad-row direction (x). The square of the ratio of the diffusion (σ) to the resolution (σ_X) gives N_{eff} from Eq. (1) with $\sigma_{X0} = 0$.

Fig. 4 shows the obtained N_{eff} and $\langle 1/N \rangle^{-1}$ as a function of σ/h . The effective number of electrons

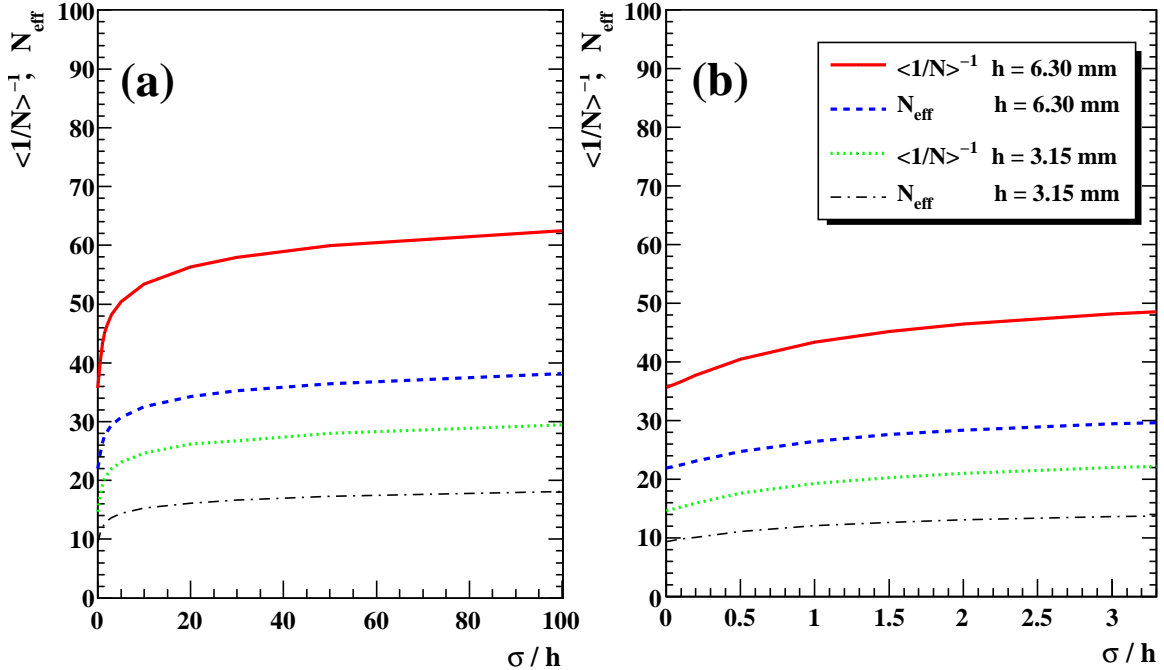


Figure 4: Inverse of the average of $1/N$ and effective number of electrons as a function of σ/h , given by the simulation for $h = 6.30 \text{ mm}$ and 3.15 mm . The values for small (realistic) σ/h are shown in (b). The relative variance of the avalanche fluctuation (f) is taken to be $2/3$. The legends are identical for (a) and (b).

certainly increases with σ/h in association with the increase of $\langle 1/N \rangle^{-1}$. The asymptotic value of

¹¹ Note that $D_x = D_y = D$ since the magnetic field (if it exists) is parallel to the z -axis.

$\langle 1/N \rangle^{-1}$ is about 70 (35) for $h = 6.3$ mm (3.15 mm) as expected. However, the increase of N_{eff} is rather slow and would be observable only for large values of σ/h , i.e. at (very) long drift distances.

Examples of the resolution squared as a function of the drift distance are shown in Fig. 5 for pad heights of 6.3 mm and 3.15 mm. The chamber gas is taken to be Ar-CF4 (3%)-isobutane (2%) as in the experiments of Refs. [5, 6]. The deviation from the linear dependence (Eq. (1) with a constant

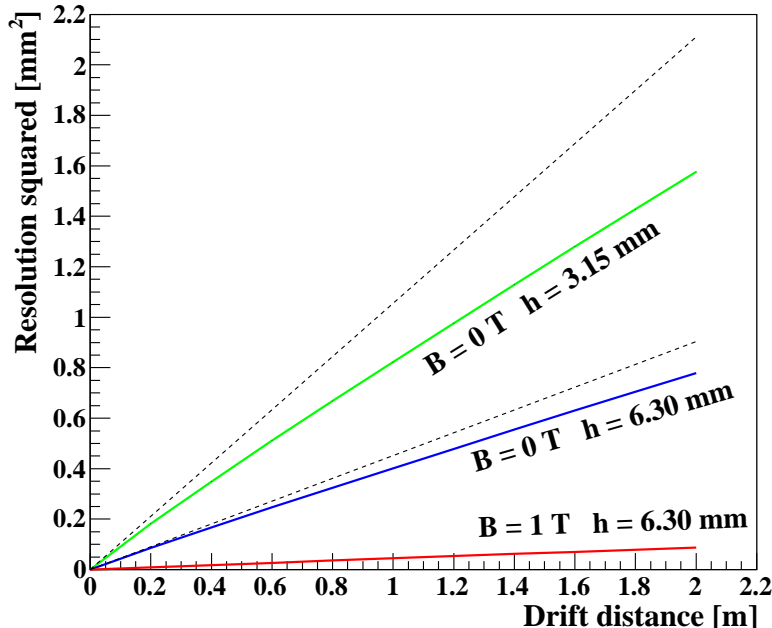


Figure 5: Resolution squared per pad row as a function of the drift distance (z) given by the simulation for $B = 0$ and 1 T, with a pad height (h) of 6.3 mm. The diffusion constant is assumed to be 315 (101) $\mu\text{m}/\sqrt{\text{cm}}$ for $B = 0$ T (1 T) given by Magboltz [7] for a gas mixture of Ar-CF4 (3%)-isobutane (2%) and a drift field of 250 V/cm. The relation simulated for $B = 0$ T with $h = 3.15$ mm is also shown for comparison. The dashed straight lines show the linear relations with the values of N_{eff} fixed to those at $z = 0$, in the case of $B = 0$ T. For $B = 1$ T, N_{eff} is almost constant throughout the drift distance shown in the figure.

N_{eff} evaluated at $z = 0$) is prominent at long drift distances without the magnetic field, in particular for the shorter pad height.

6. Conclusion

We estimated the effect of the electron diffusion normal to the pad-row direction (D_y) on the spatial resolution of TPCs operated in argon-based gas mixtures. It does affect the effective number of electrons contributing to the azimuthal coordinate measurement and thus makes N_{eff} drift-distance dependent: $N_{\text{eff}} = N_{\text{eff}}(\sigma/h) = N_{\text{eff}}(z)$ for a fixed value of h . The value of N_{eff} increases with the drift distance since the distribution of the number of electrons detected by a pad row asymptotically approaches a Poissonian by de-clustering. However, the de-clustering process is rather slow because its scaling parameter is σ/h , and N_{eff} can be assumed to be constant for practical TPCs operated under a strong axial magnetic field.

In addition, the influence of avalanche fluctuation (R_q) was found to be almost constant ($\sim 1 + f$) for a realistic pad-row pitch greater than ~ 6 mm (see Appendix A). Therefore Eq. (2) is expected to give a good approximation for the value of N_{eff} , with $\langle 1/N \rangle$ estimated assuming $D_y = 0$.

It is unlikely that the large value of N_{eff} observed with the larger TPC prototype, with a maximum drift length of ~ 600 mm and a pad-row pitch of 7 mm, arises from the finite D_y . The larger N_{eff} may have been owing to other factors such as smaller avalanche fluctuation (f), or improvement of the signal-to-noise ratio and/or better calibration of the readout electronics (see Appendix C of Ref. [5]). It should be noted that gas contaminants such as oxygen could affect the apparent value of N_{eff} as well, through the capture of electrons during their drift towards the readout plane.

The increase of N_{eff} would be observed at long drift distances with a large TPC operated in a gas with a relatively large transverse diffusion constant in the absence of magnetic field (see Fig. 5).

Acknowledgments

We would like to thank many colleagues of the LCTPC collaboration for their continuous encouragement and support, and for fruitful discussions. This work was partly supported by the Specially Promoted Research Grant No. 23000002 of Japan Society for the Promotion of Science.

Appendix A. Pad-height dependence of N_{eff}

In the previous work, the pad-row pitch (\sim pad height h) was fixed to 6.3 mm [1]. We show here the pad-height dependence of the effective number of electrons given by a numerical simulation. The simulation code is exactly the same as that developed for Ref. [1]. Therefore the diffusion of drift electrons normal to the pad-row direction (D_y) is not taken into account and the values of N_{eff} are those for zero drift distance.

If we write $N_{\text{eff}} = \langle N \rangle / R$, with R being a reduction factor, R is expressed as $R = R_N \cdot R_q$, where $R_N = \langle N \rangle \cdot \langle 1/N \rangle$ and R_q derives from the avalanche fluctuation in the detection device for each of the drift electrons [1]. The value of R_q is expected to be close to $1 + f$ for large $\langle N \rangle$ (large pad height) since $\sum_{i=1}^N q_i \sim N \cdot \langle q \rangle$ becomes a good approximation. Fig. A.1 shows the pad-height dependences of R_N , R_q and R . The relative variance of avalanche fluctuation (f) is taken to be $2/3$. The value

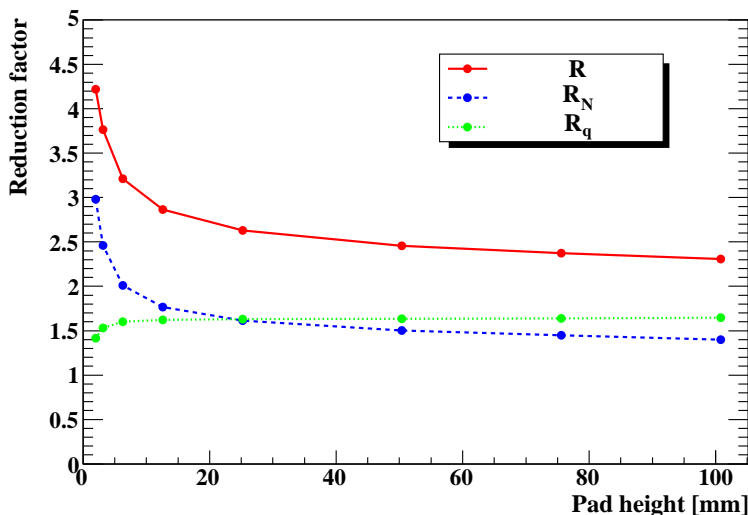


Figure A.1: Reduction factors (R , R_N and R_q) as a function of the pad height. The relative variance of avalanche fluctuation (f) is taken to be $2/3$.

of R_q is almost constant ($\sim 1 + f$) for practical pad heights ($\gtrsim 6$ mm) whereas R_N is a decreasing function of the pad height as expected.

The values of $\langle 1/N \rangle^{-1}$ ($= \langle N \rangle / R_N$) and N_{eff} are plotted in Fig. A.2 against the pad height, along with $\langle N \rangle$. It is clear that N_{eff} is not a linear function of the pad height because of R_N decreasing

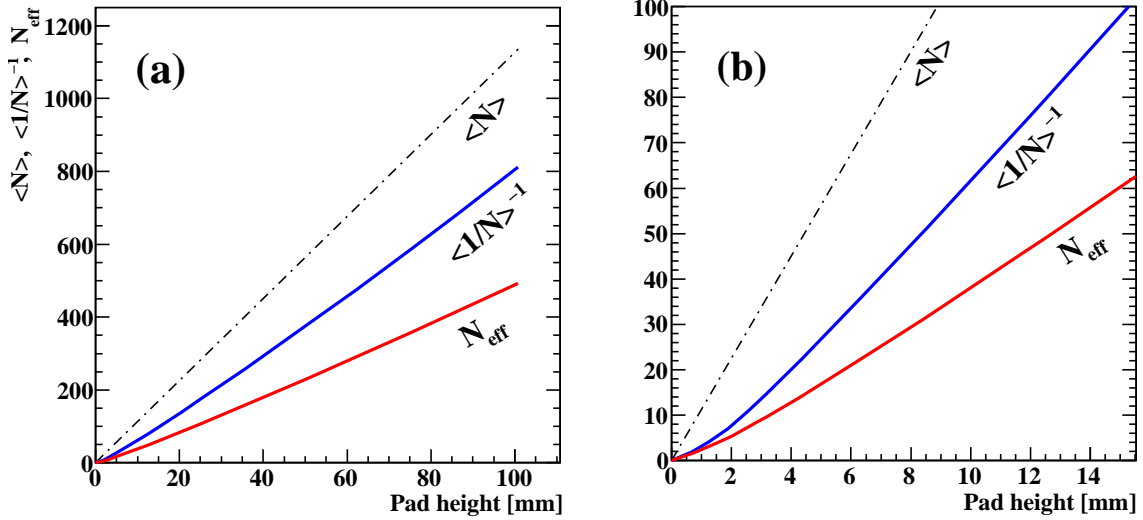


Figure A.2: (a) Average number of electrons ($\langle N \rangle$), inverse of the average of $1/N$ ($\langle 1/N \rangle^{-1}$), and effective number of electrons (N_{eff}) as a function of the pad height. (b) Details for small pad heights.

with the pad height. The effective number of electrons is about 31% (43%) of $\langle N \rangle$ for a pad height of 6.3 mm (100.8 mm).

Appendix B. Derivation of the function g

In this appendix we derive the explicit expression of the function $g(\sigma/h)$ used to evaluate $\text{Var}(\nu)$ and $\text{Var}(N)$ in Section 4. The function is defined as

$$h \cdot g\left(\frac{\sigma}{h}\right) = \lim_{H \rightarrow \infty} \int_{-H/2}^{H/2} \Pi^2(Y) dY = \int_{-\infty}^{\infty} \Pi^2(Y) dY$$

where

$$\Pi(Y) = \int_{-h/2}^{h/2} G(y; Y, \sigma) dy$$

with

$$G(y; Y, \sigma) \equiv \frac{1}{\sqrt{2\pi}\sigma} \cdot \exp\left[-\frac{(y - Y)^2}{2\sigma^2}\right].$$

Let us carry out the integration on the right hand side of the equation:

$$\begin{aligned} \int_{-\infty}^{\infty} \Pi^2(Y) dY &= \frac{1}{2\pi\sigma^2} \int_{-\infty}^{\infty} \left[\int_{-h/2}^{h/2} \exp\left(-\frac{(y - Y)^2}{2\sigma^2}\right) dy \cdot \int_{-h/2}^{h/2} \exp\left(-\frac{(y' - Y)^2}{2\sigma^2}\right) dy' \right] dY \\ &= \frac{1}{2\pi\sigma^2} \int_{-\infty}^{\infty} dY \int_{-h/2}^{h/2} dy \int_{-h/2}^{h/2} dy' \exp\left[-\frac{1}{2\sigma^2} \left((y - Y)^2 + (y' - Y)^2\right)\right] \end{aligned}$$

$$\begin{aligned}
&= \frac{1}{2\pi\sigma^2} \int_{-\infty}^{\infty} dY \int_{-h/2}^{h/2} dy \int_{-h/2}^{h/2} dy' \exp \left[-\frac{1}{\sigma^2} \left(Y - \frac{y+y'}{2} \right)^2 - \frac{1}{4\sigma^2} (y-y')^2 \right] \\
&= \frac{1}{2\sqrt{\pi}\sigma} \int_{-h/2}^{h/2} dy \int_{-h/2}^{h/2} dy' \exp \left[-\frac{1}{4\sigma^2} (y-y')^2 \right] \\
&= \frac{2}{\sqrt{\pi}\sigma} \int_0^{h/\sqrt{2}} d\xi \int_0^{h/\sqrt{2}-\xi} \exp \left(-\frac{\eta^2}{2\sigma^2} \right) d\eta \\
&\hspace{15em} \text{with } \xi = \frac{(y'+y)}{\sqrt{2}} \text{ and } \eta = \frac{(y'-y)}{\sqrt{2}} \\
&= \frac{2h}{\sqrt{\pi}} \int_0^1 du \int_0^{h \cdot (1-u)/2\sigma} \exp(-v^2) dv \\
&\hspace{15em} \text{with } u = \frac{\sqrt{2}}{h}\xi \text{ and } v = \frac{\eta}{\sqrt{2}\sigma} \\
&= h \int_0^1 f(u) du \\
&\hspace{15em} \text{with } f(u) = \frac{2}{\sqrt{\pi}} \int_0^{h \cdot (1-u)/2\sigma} \exp(-v^2) dv \\
&= h \cdot \left([uf(u)]_0^1 - \int_0^1 u f'(u) du \right) \\
&= \frac{h^2}{\sqrt{\pi}\sigma} \int_0^1 u \cdot \exp \left[-\left(\frac{h \cdot (1-u)}{2\sigma} \right)^2 \right] du \\
&= \frac{2h}{\sqrt{\pi}} \int_0^{h/2\sigma} \left(1 - \frac{2\sigma}{h} t \right) \cdot \exp(-t^2) dt \\
&\hspace{15em} \text{with } t = \frac{h \cdot (1-u)}{2\sigma} \\
&= h \cdot \left(\operatorname{erf} \left(\frac{h}{2\sigma} \right) - \frac{4\sigma}{\sqrt{\pi}h} \int_0^{h/2\sigma} t \cdot \exp(-t^2) dt \right) \\
&= h \cdot \left(\operatorname{erf} \left(\frac{h}{2\sigma} \right) - \frac{2\sigma}{\sqrt{\pi}h} \int_0^{h^2/4\sigma^2} \exp(-w) dw \right) \\
&\hspace{15em} \text{with } w = t^2 \\
&= h \cdot \left[\operatorname{erf} \left(\frac{h}{2\sigma} \right) + \frac{2\sigma}{\sqrt{\pi}h} \cdot \left(\exp \left(-\frac{h^2}{4\sigma^2} \right) - 1 \right) \right].
\end{aligned}$$

Hence,

$$g\left(\frac{\sigma}{h}\right) = \operatorname{erf}\left(\frac{h}{2\sigma}\right) - \frac{2}{\sqrt{\pi}} \cdot \frac{\sigma}{h} \cdot \left[1 - \exp\left(-\frac{h^2}{4\sigma^2}\right) \right].$$

It should be noted that the error function is given by

$$\operatorname{erf}(x) = \frac{2}{\sqrt{\pi}} \int_0^x e^{-t^2} dt$$

and that

$$g(0) = \operatorname{erf}(\infty) = 1 \quad \text{and} \quad g(\infty) = 0.$$

References

- [1] M. Kobayashi, Nucl. Instr. and Meth. A 562 (2006) 136.
- [2] W. Blum, W. Riegler and L. Rolandi, Particle Detection with Drift Chambers, Springer-Verlag, 2008.
- [3] M. Kobayashi, et al., Nucl. Instr. and Meth. A 581 (2007) 265;
M. Kobayashi, et al., Nucl. Instr. and Meth. A 584 (2008) 444.
- [4] D.C. Arogancia, et al., Nucl. Instr. and Meth. A 602 (2009) 403.
- [5] M. Kobayashi, et al., Nucl. Instr. and Meth. A 641 (2011) 37.
- [6] R. Yonamine, JINST 7 (2012) C06011.
- [7] S.F. Biagi, Nucl. Instr. and Meth. A 421 (1999) 234.